Proceedings of the 17th International Heat Transfer Conference, IHTC-17
August 14–18, 2023, Cape Town, South Africa

IHTC17 | ID: 511

ADJOINT SENSITIVITY ANALYSIS FOR HEAT TRANSFER ENHANCEMENTS IN STRUCTURED CHANNELS

David Mueller,[1,*] Yukinori Kametani,[2] Yosuke Hasegawa,[3] Alexander Stroh[1]

[1] Institute of Fluid Mechanics, KIT, Karlsruhe, Germany
[2] School of Science and Technology, Meiji University, Kawasaki, Japan
[3] Institute of Industrial Science, The University of Tokyo, Tokyo, Japan

ABSTRACT

A method for the sensitivity analysis for wall bounded thermal flows including conjugate heat transfer based on the adjoint method is proposed and implemented. In a periodic domain, the flow rate and temperature are kept constant using a uniform source. The solid region is modeled using a volume penalization approach for the velocity and by adapting the thermal diffusivity in the temperature equation. To account for an increased transport due to flow instabilities, time averaging is applied and effective diffusivities are introduced to the adjoint equations. Applied to a channel flow with rectangular obstacles, the sensitivity distribution on the wall surface is computed, showing increased sensitivities especially in regions with high temperature gradients. The obtained sensitivities allow to optimize an initial topology with respect to an objective function. Additionally, the contribution to the sensitivities resulting from different expressions in the primal equations provide insights about the transport mechanisms in the flow. The sensitivities suggest that the surface area should be increased in the regions with high heat fluxes and tend to modify the geometry hindering the occurrence of the flow separation.

KEY WORDS: conjugate heat transfer, adjoint method, sensitivity analysis

1. INTRODUCTION

Optimization of engineering systems can significantly improve their performance, functionality, and cost-effectiveness, and also minimize their environmental impact, making it a crucial area of research. Optimizing the shape of objects in the aerospace and automotive industries and the design of structures and manufacturing processes are some of the most common optimization tasks. In the present work we consider an adjoint-based sensitivity evaluation [1] for a generic fluidic system – a flow through a structured channel – with an aim to improve thermohydraulic efficiency of the channel via adjustment of structuring shape. The adjoint method constitutes a mathematical tool that can be used to efficiently compute the sensitivity of a quantity of interest with respect to the design variables. The method presents several advantages over other optimization methods, including its ability to efficiently handle large-scale design problems and complex constraints and objectives [2].

We consider a generic heat exchanger – 2D periodic laminar flow of an incompressible fluid through a structured channel under constant flow rate condition as shown in Fig. 1. Similarly, the heat transfer is considered by taking into account the temperature field treated as passive scalar with a uniform heat source to prescribe a constant bulk temperature in the system. In such configuration the total drag (which is proportional to the

*Corresponding David Mueller: david.mueller@kit.edu

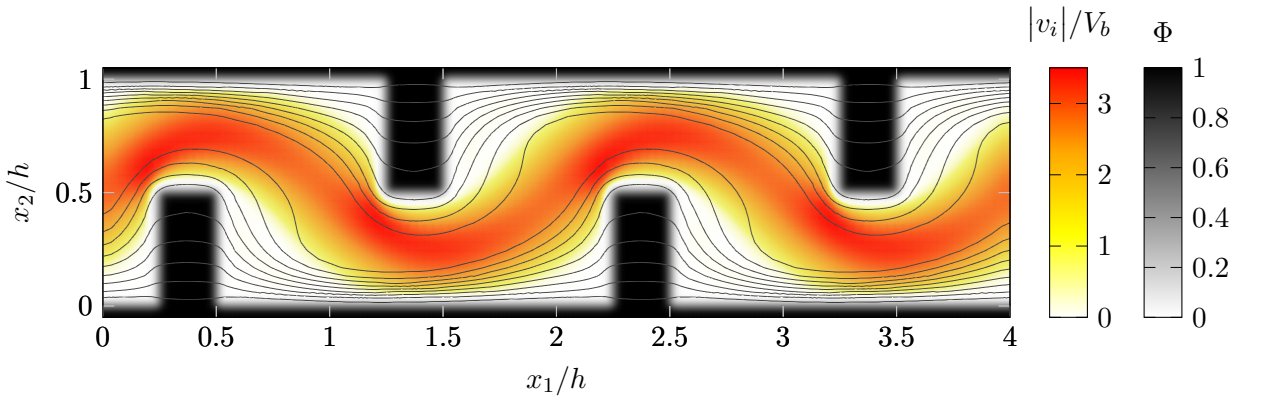

Fig. 1 Velocity magnitude distribution and indicator function in the considered laminar structured channel. Black iso-contours show the temperature distribution with a step of $0.15T_b$.

energy needed to pump the fluid through the channel) is characterized using drag coefficient C_f and the heat transfer performance is estimated using Stanton number St. The ultimate goal is, however, to achieve a higher heat transfer rate (St) with the least total drag (C_f) - also called *dissimilar* heat transfer enhancement [3, 4]. In spite of the challenges due to the strong similarity between momentum and heat transfer, the concept of dissimilar enhancement has been successfully implemented using fins [5, 6], dimples [7] and vortex generators [8]. In the context of heat exchangers the adjoint technique has been successfully applied for shape optimization of fins in pin-fin-array heat exchangers yielding a significant increase in thermohydraulic efficiency accompanied by a reduction in size and amount of material needed for manufacturing [9, 10]. Nonetheless, the optimization is often seen as a result-oriented tool, so the physical explanation of the reasons for a better shape performance remain out of the scope of the studies. In the present work we aim to shed light on the underlying mechanism behind the adjoint-based sensitivity analysis in order to better understand the interaction between the shape or shape adjustment and its effect on the physics of the fluid flow.

2. METHODOLODY

2.1 Heat transfer in structured channels

2.1.1 Governing equations The incompressible, laminar flow of a uniformly heated fluid through a structured channel is numerically investigated in this study. Using the adjoint method [1], the sensitivities describing the excepted change in an objective functional with respect to a change the design variable Ψ, i.e. in the channel's topology, are computed and discussed. The flow is driven by a pressure gradient which is adapted to maintain a specified bulk velocity V_b. Analogously, the fluid is heated with a uniform heat source to sustain the prescribed the bulk temperature T_b. The solid region is identified using an indicator function (see section 2.1.2). An immersed boundary method (IBM) models the structures by using a momentum sink to prescribe the no-slip boundary condition at the solid/fluid boundary and enforce zero velocity within the solid region. Conjugate heat transfer is considered by adapting the thermal diffusivity utilizing the indicator function Φ. Depending on the prescribed Reynolds number $Re = V_b h/\nu$, with the channel height h and kinematic viscosity ν, transient phenomena such as vortex shedding can occur, increasing the effective viscosity and heat flux locally.

The physical behavior of the flow is described by the conservation laws for mass (1), momentum (2) and energy (3), which reduces to the passive scalar equation for temperature:

$$R^p = -\frac{\partial v_j}{\partial x_j}, \tag{1}$$

$$R_i^v = \frac{\partial v_i}{\partial t} + \frac{\partial (v_i v_j)}{\partial x_j} + \frac{\partial p}{\partial x_i} + (1-\Phi)\, m_{v,i} - \frac{\partial}{\partial x_j}\left[\nu\left(\frac{\partial v_i}{\partial x_j} + \frac{\partial v_j}{\partial x_i}\right)\right] + \Phi\eta v_i, \tag{2}$$

$$R^T = \frac{\partial T}{\partial t} + v_j \frac{\partial T}{\partial x_j} + (1-\Phi)\, q_v - \frac{\partial}{\partial x_j}\left[\left(\Phi\, \alpha_s + (1-\Phi)\, \alpha_f\right)\frac{\partial T}{\partial x_j}\right]. \tag{3}$$

In Eqn. (1) − (3), p, v_i and T denote the pressure, the velocity and the temperature, respectively. $\Phi = f(\Psi)$ is the indicator function where $\Phi = 1$ refers to the solid and $\Phi = 0$ to the fluid region, while α_s and α_f are the respective thermal diffusivities of the solid and fluid region. $m_{v,i}$ and q_v are the driving sources applied to the fluid domain to maintain the respective bulk values. Similarly to the method proposed by Goldstein, Handler and Sirovich [11], η is a proportional coefficient for the volume penalization in the solid region. It is typically a large, positive value that is chosen empirically, since overly large values can cause numerical instabilities. The left hand side of Eqn. (1) - (3), R^p, R_i^v and R^T are zero by definition.

In the 2D domain, periodic boundary conditions for the in- and outlet are used for v_i, p and T. At the walls, v_i and T are set to zero. Hence, T is considered the temperature difference between the wall and the fluid. For p, a zero gradient condition is applied. Additionally, the indicator function is chosen as $\Phi = 1$ at the wall. In the context of the adjoint method, Eqn. (1) - (3) induce constraints to the optimization problem: the respective fields are required to fulfill the conservation laws. Hence, we take into account that a change in the topology should not lead to unrealistic behavior of the thermofluid when determining sensitivities. Since constant V_b and T_b are prescribed using the adaptive momentum and heat source, two additional constraints are required:

$$R_i^m = \int_\Omega (1-\Phi)\,(v_i - n_i\, V_b)\; dV, \tag{4}$$

$$R^h = \int_\Omega (1-\Phi)\,(T - T_b)\; dV. \tag{5}$$

Eqn. (4) and (5) describe the above mentioned condition for v_i and T in the fluid domain. The vector n_i points in the main direction of the flow. From a mathematical perspective, $(v_i, p, T, m_{v,i}, q_v, \Psi)$ are the variables of the optimization problem the sensitivities are computed for. To fulfill the constraints (1) - (5), only the design variable Ψ expressing the topology can be chosen independently. Consequently, $(v_i, p, T, m_{v,i}, q_v)$ are referred to as the primal variables.

2.1.2 Smoothed-interface immersed boundary method In the previous section, the indicator function Φ is introduced as a function of the design variable $\Phi = f(\Psi)$. Throughout this study, a level set function [12] is used as the design variable. It is defined as the signed distance to the fluid-solid-interface. Hence, positive values of Ψ refer to the solid region, the zero-level implicitly defines the wall and negative values refer to the fluid region. Since $f(\Psi)$ is required to be differentiable, the smoothing-parameter Δ is introduced to compute Φ using Eqn. (6) as depicted in Fig. 2.

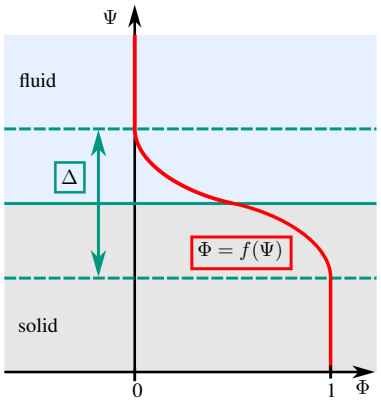

$$\Phi(\Psi) = \begin{cases} 0, & \Psi \leq -\frac{\Delta}{2}, \\ \frac{1}{2}\left[\sin\left(\frac{\pi\Psi}{\Delta}\right) + 1\right], & |\Psi| < \frac{\Delta}{2}, \\ 1, & \Psi \geq \frac{\Delta}{2} \end{cases} \tag{6}$$

Fig. 2 The indicator function has a smooth transition area Δ in the vicinity of the interface [10].

2.1.3 Effective diffusivities Depending on the Reynolds number Re and the shape of the solid structure, vortex shedding can be observed in the considered flow, increasing the effective momentum- and heat fluxes in the wake. To take this into account, Reynolds decomposition can be applied, so the instantaneous flow quantities are split into mean values and fluctuations $\phi = \overline{\phi} + \phi'$ and averaged in time during the numerical simulation. Using Boussinesq hypothesis, the additional momentum fluxes from the transient behavior, i.e. the Reynolds stresses, are approximated using the scalar eddy viscosity ν_b and the time averaged velocity gradients:

$$\frac{\partial \overline{v_i' v_j'}}{\partial x_j} = \frac{\partial a_{ij}}{\partial x_j} + \frac{2}{3}\frac{\partial (k\delta_{ij})}{\partial x_j} \approx -\frac{\partial}{\partial x_j}\left[\nu_b\left(\frac{\partial \overline{v_i}}{\partial x_j} + \frac{\partial \overline{v_j}}{\partial x_i}\right)\right] + \frac{2}{3}\frac{\partial k}{\partial x_i}. \tag{7}$$

Analogously, the thermal eddy diffusivity α_b is introduced:

$$\frac{\partial \overline{v_j' T'}}{\partial x_j} \approx -\frac{\partial}{\partial x_j}\left[\alpha_b \frac{\partial \overline{T}}{\partial x_j}\right]. \tag{8}$$

Since only ν_b and α_b are unknown, Eqn. (7) and (8) are used to determine both quantities.

2.2 Objective functions

2.2.1 Stanton number With the aim to increase the efficiency of heat exchangers, choosing the maximization of the Stanton number as the objective is straightforward. For the described configuration, the Stanton number is defined as

$$St = \frac{Nu}{Re\,Pr} = \frac{1}{T_b\,V_b}\,\frac{1}{L_x\,L_z}\int_\Omega (1-\Phi)\,q_v\,dV, \tag{9}$$

where L_x and L_z are the length and the height of the computational domain. Since the multiplication with a constant value does not influence the optimal topology, Eqn. (9) shows that maximizing for the Stanton number is equivalent to maximizing the primal variable q_v and the objective function can be chosen as $J_{St} = -T_b V_b L_x L_z St$.

2.2.2 Skin friction Higher flow rates are associated with higher pumping power needed for fluid transport through the channel. Hence, considering the skin friction coefficient C_f besides St might be also essential for the design of an efficient heat exchanger. C_f is computed using the primal variable $m_{v,i}$ and the flow direction n_i associated with V_b:

$$C_f = \frac{2\,\tau_w}{\rho\,V_b^2} = \frac{2\,\delta\,\Delta P}{\rho\,V_b^2\,L_x} = n_i\frac{2\,\delta}{V_b^2}m_{v,i} = \frac{2}{V_b^2\,L_x L_z}\int_\Omega n_i(1-\Phi)\,m_{v,i}\,dV. \tag{10}$$

The C_f-based objective $J_{C_f} = V_b^2 L_x L_z$ is formally identical to J_{St} except for the positive sign indicating the minimization of C_f.

2.2.3 Reynolds analogy Combining St and C_f, an objective based on the Reynolds analogy factor Ra considers both the gain with respect to heat transfer and the momentum loss. Starting from Ra, a generalized objective can be derived as presented in the following section:

$$Ra = \frac{2\,St}{C_f} = \frac{V_b}{T_b}\int_\Omega (1-\Phi)\,q_v\,dV\left[\int_\Omega n_i(1-\Phi)\,m_{v,i}\,dV\right]^{-1}. \tag{11}$$

2.3 Adjoint sensitivity analysis

2.3.1 Adjoint variables Since the adjoint method is based on the augmented Lagrangian method [13], each constraint to the optimization problem introduces a Lagrangian multiplier in the Lagrangian function (see section 2.3.2). Throughout the following procedure, these Lagrangian multipliers are referred to as the adjoint variables. From the equality constraints (1) - (3) the adjoint pressure field q, the adjoint velocity field u_i and the adjoint temperature field Θ arise. As for the primal variables, the constraints (4) and (5) lead to a single adjoint momentum source λ^m and a single adjoint heat source λ^h, which are no field quantities. In this context we refer to $(u_i, q, \Theta, \lambda_i^m, \lambda^h)$ as adjoint variables.

2.3.2 Definition of the Lagrangian Following the procedure for the augmented lagrangian method, the lagrangian function is introduced:

$$L = J + \frac{\lambda_i^m}{V_b} R_i^m + \frac{\lambda^h}{T_b}\overline{R^h} + \int_\Omega \frac{q}{V_b}\overline{R^p} dV + \int_\Omega \frac{u_i}{V_b}\overline{R_i^v} dV + \int_\Omega \frac{\Theta}{T_b}\overline{R^T} dV \,. \tag{12}$$

In Eqn. (12), J is a generic objective function and $\overline{R_i^v} = \overline{R^h} = \overline{R^p} = \overline{R^T} = \overline{R_i^v} = 0$ are the time averaged equality constraints. To avoid numerical issues due to different orders of magnitudes in the values of the flow quantities, the constraints are scaled with either V_b or T_b.

2.3.3 Derivation of the adjoint equations The derivative of the lagrangian defined in Eqn. (12) depends on the unknown partial derivatives of the primal variables with respect to the design variable. Using the chain and product rules as well as partial integration, the derivative of Eqn. (12) can be expressed as a linear combination of the partial derivatives, the partial derivative of Φ and surface integrals:

$$\begin{aligned}
\frac{\partial L}{\partial \Psi} = {} & \frac{1}{V_b}\Bigg[\underbrace{-\frac{\partial u_i}{\partial x_j}}_{Q^p}\Bigg]\frac{\partial p}{\partial \Psi} + \frac{1}{T_b}\Bigg[\underbrace{-v_j\frac{\partial \Theta}{\partial x_j} - \frac{\partial}{\partial x_j}\left[\alpha\frac{\partial \Theta}{\partial x_j}\right] + \lambda^h(1-\Phi)}_{Q^T}\Bigg]\frac{\partial T}{\partial \Psi} \\
& + \frac{1}{V_b}\Bigg[\underbrace{\frac{\partial q}{\partial x_i} + \lambda_i^m(1-\Phi) - v_j\frac{\partial u_i}{\partial x_j} - \frac{\partial}{\partial x_j}\left[\nu\left(\frac{\partial u_i}{\partial x_j} + \frac{\partial u_j}{\partial x_i}\right)\right] + \eta u_i \Phi + u_j\frac{\partial v_j}{\partial x_i} + \frac{\Theta}{T_b}\frac{\partial T}{\partial x_j}V_b}_{Q_i^v}\Bigg]\frac{\partial v_i}{\partial \Psi} \\
& + \underbrace{\int_\Omega \left(n_i V_b c^{J,P} - u_i\right)(1-\Phi)\, dV}_{Q_i^m}\frac{\partial^2 P}{\partial \Psi \partial x_i} + \underbrace{\int_\Omega \left(T_b c^{J,q} - \Theta\right)(1-\Phi)\, dV}_{Q^h}\frac{\partial q_v}{\partial \Psi} + \underbrace{s\frac{\partial \Phi}{\partial \Psi}}_{\text{sensitivity}} + \int_{\partial\Omega}(...)\, dA.
\end{aligned} \tag{13}$$

All quantities in Eqn. (13) are time averaged. In Eqn. (13), $c^{J,P}$ and $c^{J,q}$ are constant coefficients arising from the generalized objective presented in the next section. To compute the sensitivities independently of the partial derivatives of the primal variables, the adjoint variables are determined from the condition that $Q_i^v = Q^h = Q^p = Q^T = Q_i^v = 0$. The adjoint boundary conditions are obtained from the surface integral in Eqn. (13). For the investigated setup, the adjoint boundary conditions coincide with the boundary conditions for the primal field variables. If the adjoint equations are fulfilled, the sensitivities are computed as

$$s = \frac{1}{V_b}\Bigg[\eta u_i v_i + m_{v,i}(u_i - n_i U_b) + \lambda_i^m(v_i - n_i V_b)\Bigg] + \frac{1}{T_b}\Bigg[\Delta_\alpha \frac{\partial \Theta}{\partial x_j}\frac{\partial T}{\partial x_j} + q_v(\Theta - \Theta_b) + \lambda^h(T - T_b)\Bigg] \tag{14}$$

with $\Delta_\alpha = \alpha_s - \alpha_f$. The expression for the sensitivities in Eqn. (14) is not independent of the objective function. According to Q_i^m and Q^h, the adjoint bulk velocity U_b and adjoint bulk temperature Θ_b are determined from the objective. However, in the proposed framework the objective can be changed by updating U_b and Θ_b.

2.3.4 Generalized objective The differentiation of the objectives presented in section 2.2 can be generalized as presented in Eqn. (15). The derivative for J_{St} is obtained by choosing $c^{J,q} = 1$ and $c^{J,P} = 0$ leading to $\Theta_b = -V_b$ and $U_b = 0$. J_{C_f} is obtained with $c^{J,q} = 0$ and $c^{J,P} = 1$, resulting in $\Theta_b = 0$ and $U_b = V_b$:

$$\begin{aligned}\frac{\partial J}{\partial \Psi} =& c^{J,P} \int_\Omega n_i (1-\Phi) \frac{\partial^2 P}{\partial \Psi \, \partial x_i} \, dV - c^{J,P} \int_\Omega n_i m_{v,i} \frac{\partial \Phi}{\partial \Psi} \, dV \\ & - c^{J,q} \int_\Omega (1-\Phi) \frac{\partial q_v}{\partial \Psi} \, dV + c^{J,q} \int_\Omega q_v \frac{\partial \Phi}{\partial \Psi} \, dV.\end{aligned} \tag{15}$$

2.3.5 Frozen effective diffusivities The effective diffusivities arising from the time averaging procedure presented in section 2.1.3 depend on the distance to the wall i.e. the design variable. Similarly to the frozen turbulence assumption [14], the partial derivatives of the effective diffusivities are neglected throughout this study.

3. PROCEDURE

3.1 Computational domain and flow configuration

In the present study, a two-dimensional domain of the size $L_x/h = 4$ and $L_y/h = 1.1$ is considered. The domain is discretized with a uniform cell size of $\Delta x/h = 0.0005$. For the time integration, an adaptive time step is used, ensuring a maximum cell based Courrant number of $Co = v_i \Delta t/\Delta x = 0.5$. The shape of the solid structure is shown in Fig. 1. The thin layer of solid at the top and bottom wall has a thickness of $0.05h$. The spacing in between adjacent obstacles at the bottom and top wall is h, so four obstacles are placed within the periodic domain. The height of an obstacle is $0.5h$ and the width is $0.25h$. The radius of the rounded corner at the centerline of the channel is $r_{obs} = 0.0575h$. For the smoothed solid-fluid-interface, the smoothing parameter is set to $\Delta = 3\,\Delta x$. The fluid viscosity and thermal diffusivity are chosen as $\nu = \alpha_f = 10^{-5}\,\mathrm{m^2/s}$, while the solid thermal diffusivity is $\alpha_s = 10\alpha_f$. The flow is investigated at two different Reynolds numbers $Re = V_b h/\nu = [40, 80]$. At Re = 40 the flow converges to a steady state solution, whereas at $Re = 80$ vortex shedding is expected to occur.

3.2 Solution algorithm

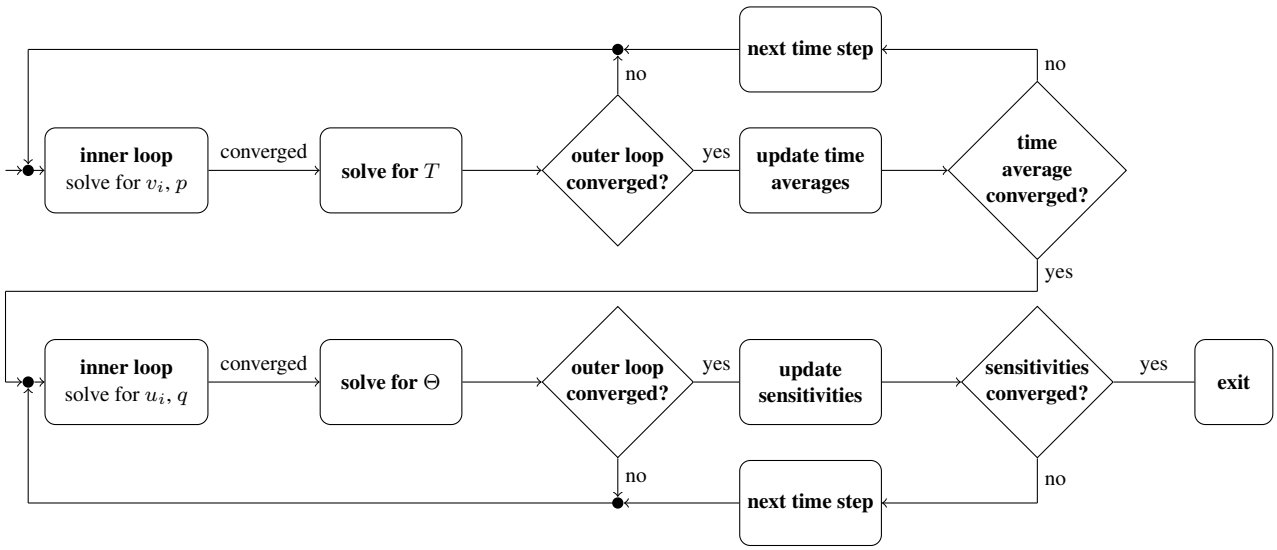

Fig. 3 Flow diagram of the solution algorithm.

The framework for the computation of sensitivities using the adjoint method is implemented in an OpenFOAM-based in-house solver utilizing the PIMPLE-algorithm for both the primal and the adjoint equations. The flow diagram of solution algorithm is depicted in Fig. 3. The primal equations are solved until a convergence criteria based on the time averaged flow quantities is met. Hence, the procedure is applicable to both steady and unsteady flow problems. During the simulation, the heat and momentum source terms are adapted to maintain the specified respective bulk value. While updating the time averaged quantities, the effective eddy viscosity and thermal diffusivity are computed. For solving the adjoint equations, the negative mean velocity is used in the adjoint convective term. Thus, the adjoint equation always describe a steady state. Analogously to the primal equations, the adjoint heat and momentum source are updated depending on the chosen objective function. The adjoint equations are solved until the sensitivities converge.

4. RESULTS

4.1 Effect of simulation domain length

As previously mentioned, the flow becomes non-stationary when Reynolds number is increased from $Re = 40$ to $Re = 80$ within the same periodic computational domain. At $Re = 80$, vortex shedding occurs at the leading corner of the rectangular obstacles and the resultant vortices interact with the obstacles downstream forming a more complex flow pattern. To compare the influence of the domain length on the results due to the propagation of this effect, an additional simulation with $L_x/h = 2$ instead of $L_x/h = 4$ is carried out. The frequency analysis of wall-normal velocity is presented in Fig. 4. On the channel centerline, at $x = 0.125h$ and $x = 1.125h$, the wall-normal velocity component v_2 is investigated. A fast Fourier transformation of the velocity shows twice as many frequency peaks for $L_x = 4h$ then for $L_x = 2h$. This confirms, that the length of the domain affects both the velocity and temperature fluctuations and thus the computed sensitivities. Consequently, the sensitivities can differ at each obstacle in the resolved flow at $Re = 80$ in the longer domain.

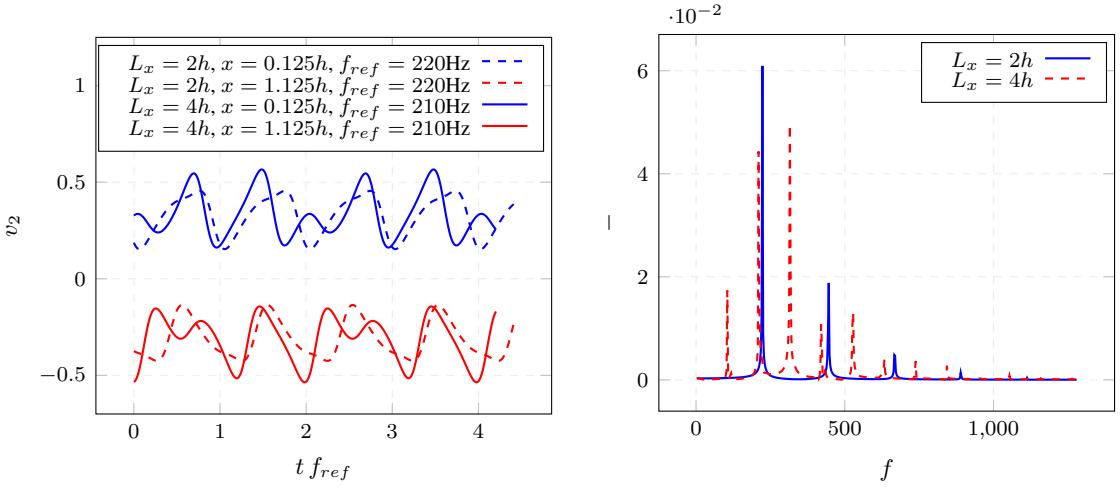

Fig. 4 Velocity $v_2(x, y = h/2)$ in time (left) and frequency (right) domain. x is the streamwise coordinate and f_{ref} is the dominant frequency.

4.2 Primal and adjoint variables

Fig. 5 shows the primal velocity magnitude and temperature in the shorter domain ($L_x = 2h$). At $Re = 40$, the flow is steady state and does not depend on the domain size. Both fields differ qualitatively due to the treatment of the IBM. In the case of the velocity field, the momentum sink reduces the velocity within the solid region to approximately zero and the reduced cross-sectional area causes an acceleration of the flow between the elements and the opposing wall. Consequently, the velocity gradients at the leading corner of the obstacles

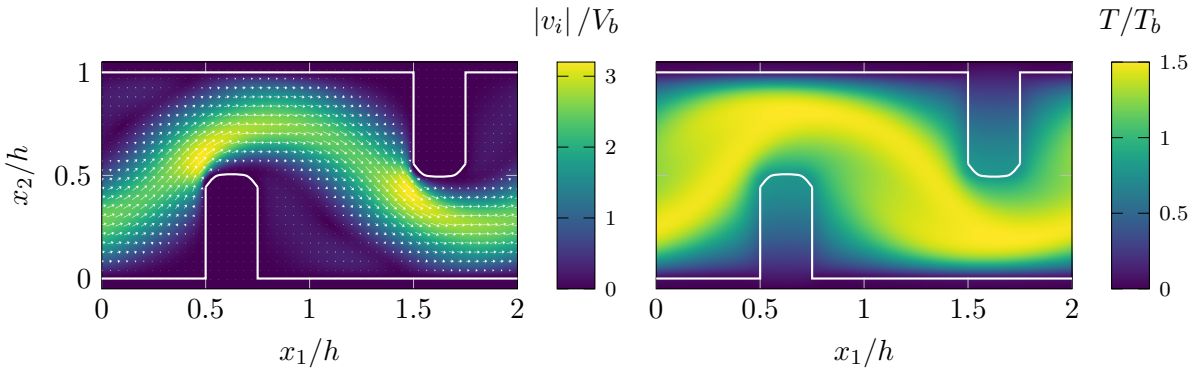

Fig. 5 Primal velocity (left) and temperature (right). White line marks the fluid/solid interface.

are very high. Behind the obstacles, a steady recirculation area forms. Due to the conjugate heat transfer, the temperature gradients at the tips are comparably small. Since uniform heating is applied to the fluid region, the temperature in the recirculation area is overestimated compared to configurations, where the heat would be provided through either convection or e.g. chemical reactions. The high momentum streak is redirected from the opposing wall towards the subsequent obstacle, so the velocity gradients in these areas are smaller than at the tips. However, heat is convectively transported close to the wall, resulting in high temperature gradients.

Choosing the maximization of Stanton number as the objective, the adjoint bulk velocity is $U_b = 0$ and the adjoint bulk temperature is $\Theta_b = -V_b$. The transpose convective terms, especially the one resulting from the temperature equation, in the adjoint velocity equation (see Eqn. (13)) acts as a driving source which is balanced by the adjoint momentum source λ^m. Consequently, vortex-like closed structures emerge as shown in Fig. 6. Since the adjoint momentum source enforces $U_b = 0$, the influence of the thermal transposed convective term to the sensivitivies via the adjoint velocity u_i is indicated by these vortices. The adjoint temperature is similar to the primal temperature except for the negative bulk value and the negative convective term. As a result of the latter, the magnitude of the adjoint temperature behind the obstacles is comparably large and the gradients of the adjoint temperature field are larger than the gradients of the temperature field in this region.

4.3 Sensitivities

The sensitivities presented in this section are computed with the previously introduced primal and adjoint fields for the Stanton number objective. The sensitivities are computed with Eqn. (14). The lower right plot in Fig. 7 shows the contribution from the change in diffusivity from the fluid to the solid region. It shows high values, where both the primal and the adjoint temperature gradients are high and thus aims to increase the thermal

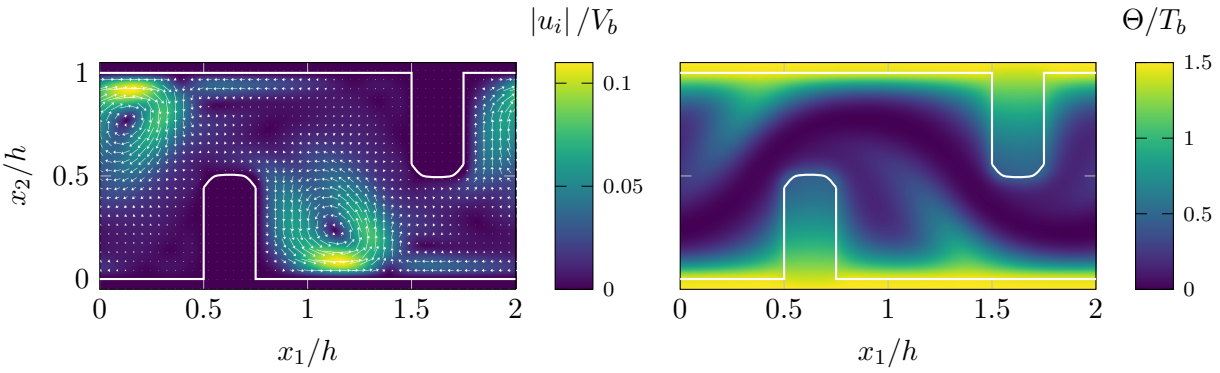

Fig. 6 Adjoint velocity (left) and adjoint temperature (right). White line marks the fluid/solid interface.

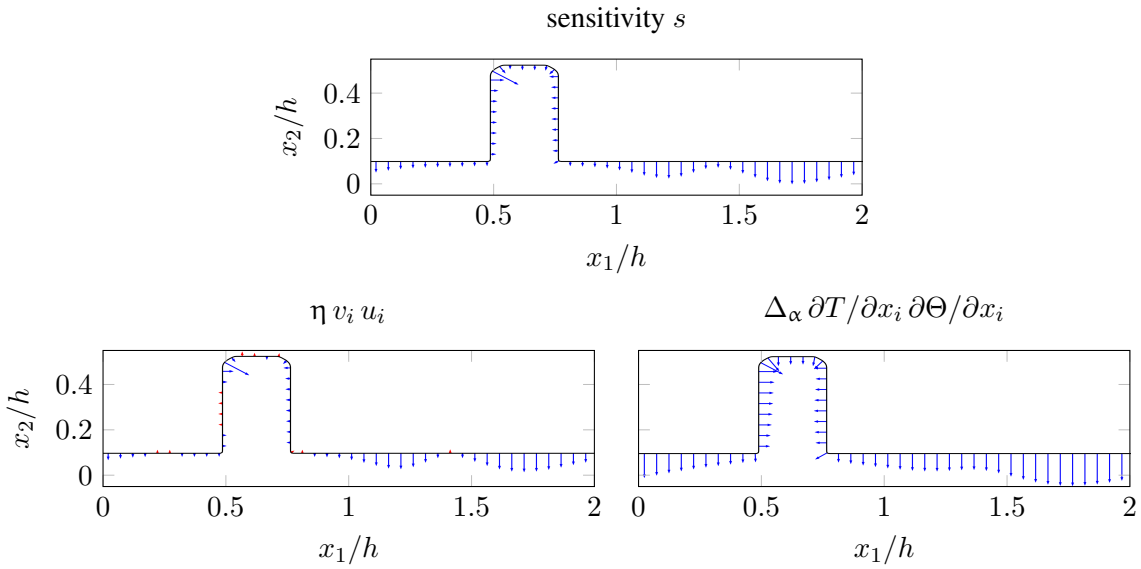

Fig. 7 Sensitivities computed for the St-objective function and the contributions from the solid model for momentum , $\eta\, v_i\, u_i$, and heat transfer, $\Delta_\alpha\, \partial T/\partial x_i\, \partial \Theta/\partial x_i$, according to Eqn. (14).

diffusivity in regions with high heat fluxes. As mentioned before, the adjoint temperature gradient is increased directly behind the obstacle and decreased further downstream compared to the gradients of the temperature field. This effect is enhanced by the circulation of the vortex. Since adding solid in the area of increased adjoint temperature gradients would decrease the circulation, the respective sensitivities indicate the benefit from removing the insulating vortex. As heat is transferred from the fluid to the wall only, the contribution from those effects will only suggest increasing the solid volume. However, combined with a constant volume constraint, the decrease in sensitivity downstream can result in the removal of solid. The lower left plot in Fig. 7 shows the sensitivity expression resulting from the IBM. It exhibits both positive and negative values. The positive value at the leading tip suggests a shape update to avoid the detachment of the flow, which would drastically increase the temperature gradient at the top respective the bottom of the obstacles. With the same reasoning, adding solid at the indicated regions at the channel's wall increases the heat transfer due to heat convection.

5. CONCLUSION

In the present study, an adjoint based method for the sensitivity analysis for thermal channel flows considering conjugate heat transfer is presented, implemented in OpenFOAM and applied to a generic configuration with rectangular obstacles. The method is derived for unsteady laminar flows and skin friction or heat transfer related objective functions in periodic domains. To implicitly define solid structures, an IBM with volume penalization based on a level set function is used. To deal with transient effects, the primal fields are time averaged and the resulting adjoint equations are closed using Boussinesq approximation. The respective effective diffusivities are computed from the known first and second moments of the primal fields. The procedure is formally identical for laminar and turbulent flows, provided a direct numerical simulation of the turbulent flow is carried out.

A generalized objective function based on volume integrals and the constraint of constant bulk values is derived for thermal wall bounded flows. However, the described approach can easily be extended, e.g. for reacting flows. The developed method is applied to a channel flow configuration with rectangular obstacles considering different Reynolds numbers for steady and unsteady laminar flows. The transient behavior of the flow is investigated depending on the domain size. The results show more complex flow patterns emerge for longer domains. Since the computation of the effective diffusivities is not trivial for complex flows, the sensitivity

analysis is firstly carried out for a steady flow at $Re = 40$. The results for the primal, adjoint and sensitivity fields are discussed and physical mechanisms that effect heat transfer are related to the results of the sensitivity analysis. For the considered configuration, the sensitivities indicate topology changes due to convective and diffusive effects. Convection is mainly relevant for the sensitivities behind the structure, where the heat transfer is inhibited by the recirculation vortex. The suggested topology change suppresses this recirculation. Diffusion plays an important role at the tips of the obstacles and at the opposing walls, where both the velocity and temperature gradients are high. In summary, optimizing for higher St, the computed sensitivities for the currently considered geometry suggest a topology update aiming at avoidance of flow separation and exposition of the solid structure to high temperature gradients.

In future work, various methods for computing the sensitivities for transient flows will be compared, and sensitivity analysis will be performed for flows with higher Reynolds numbers. Additionally, the impact of domain length on the flow, effective diffusivities, and sensitivities will be further studied. Finally, the suggested algorithm will be used to determine the optimal shape for different objective functions.

6. ACKOWLEDGEMENT

D.M. and A.S. gratefully acknowledge financial support by the Federal Ministry of Education and Research (BMBF) within the H2Giga/StacIE project.

REFERENCES

[1] Pironneau, O. (1973) On optimum profiles in Stokes flow. *Journal of Fluid Mechanics,* **59**(1), 117–128.

[2] Giannakoglou, K. and Papadimitriou, K. (2008) Adjoint methods for shape optimization. *Optimization and computational fluid dynamics,* pp. 79–108.

[3] Kasagi, N., Hasegawa, Y., Fukagata, K., and Iwamoto, K. (2012) Control of Turbulent Transport: Less Friction and More Heat Transfer. *Journal of Heat Transfer,* **134**(3).

[4] Bejan, A. (2013) Convection heat transfer, John wiley & sons, .

[5] Manglik, R. and Bergles, A. (1995) Heat transfer and pressure drop correlations for the rectangular offset strip fin compact heat exchanger. *Experimental Thermal and Fluid Science,* **10**(2), 171–180.

[6] Kays, W. and London, A. (1984) Compact heat exchangers, Krieger Pub. Co., .

[7] Elyyan, M., Rozati, A., and Tafti, D. (2008) Investigation of dimpled fins for heat transfer enhancement in compact heat exchangers. *International Journal of Heat and Mass Transfer,* **51**(11-12), 2950–2966.

[8] Fiebig, M. (1995) Vortex generators for compact heat exchangers. *Journal of Enhanced Heat Transfer,* **2**(1-2).

[9] Bacellar, D., Aute, V., Huang, Z., and Radermacher, R. (2017) Design optimization and validation of high-performance heat exchangers using approximation assisted optimization and additive manufacturing. *Science and Technology for the Built Environment,* **23**(6), 896–911.

[10] Kametani, Y. (2020) A new framework for design and validation of complex heat transfer surfaces based on adjoint optimization and rapid prototyping technologies. *Journal of Thermal Science and Technology,* **15**(2).

[11] Goldstein, D., Handler, R., and Sirovich, L. (1993) Modeling a no-slip flow boundary with an external force field. *Journal of computational physics,* **105**(2), 354–366.

[12] Osher, S. and Sethian, J. (1988) Fronts propagating with curvature-dependent speed: Algorithms based on Hamilton-Jacobi formulations. *Journal of computational physics,* **79**(1), 12–49.

[13] Nocedal, J. and Wright, S. (1999) Numerical optimization, Springer, .

[14] Anderson, W. and Venkatakrishnan, V. (1999) Aerodynamic design optimization on unstructured grids with a continuous adjoint formulation. *Computers & Fluids,* **28**(4-5), 443–480.